Construction of 3D lanthanide based MOFs with pores decorated with basic imidazole groups for selective capture and chemical fixation of CO_2

Sandeep Singh Dhankhar and C. M. Nagaraja*

Department of Chemistry, Indian Institute of Technology Ropar, Rupnagar 140001,

Punjab, India. Tel: 91- 1881-242229, Email: cmnraja@iitrpr.ac.in

Contents:

Table S2. Selected hydrogen bonding geometry (Å, °) for MOF**1** (Tb^{+3}).

Table S3. Selected bond lengths (Å) and angles (°) for MOF**2** (Sm^{+3}).

Table S4. Selected hydrogen bonding geometry (Å, °) for MOF**2** (Sm^{+3}).

Table S5. Selected bond lengths (Å) and angles (°) for MOF**3** (Eu^{+3}).

Table S6. Selected hydrogen bonding geometry (Å, °) for MOF**3** (Eu^{+3}).

Figure S4. Pore pictures of MOF**1** (Tb^{+3}) showing pore size of 1D channels before and after interpenetration.

Figure S5. Thermogravimetric analysis of MOF**1-3** (where 1 = Tb^{+3}, 2 = Sm^{+3} and 3 = Eu^{+3}) and activated MOF**1-3**.

Figure S6. N_2 adsorption-desorption isotherms of MOF**1'** (Tb^{+3}) carried out at 77K.

Figure S7. CO_2 adsorption isotherm for MOF**1'**(Tb^{+3}) at 273 K (the solid line shows the best fit to the data using Langmuir- Freundlich equation).

Figure S8. CO_2 adsorption isotherm for MOF**1'**(Tb^{+3}) at 298 K (the solid line shows the best fit to the data using Langmuir-Freundlich equation).

Figure S9. Enthalpy of CO_2 adsorption for MOF**1'**(Tb^{+3}) calculated using Clausius-Clapeyron equation.

Table S7. Comparison ofisosteric heat of adsorption (Q_{st}) values of CO_2 with various reported lanthanides MOFs.

Figure S10. Binary mixture adsorption isotherms and selectivity for CO_2/N_2 (15/85) mixtures at 273 K and 1 bar pressure obtained from IAST.

Table S8. Summary of parameters for DSLF isotherm fits.

Figure S11. Dual site Langmuir-Freundlich fitting (red line) for CO_2 adsorption isotherms collected at 273 K and up to 1 bar pressure.

Figure S12. Dual site Langmuir-Freundlich fitting (red line) for N_2 adsorption isotherms collected at 273 K and up to 1 bar pressure.

Table S9. Optimization ofcycloaddition of CO_2 with ECH catalyzed by MOF**1'**.

Figure S13. ^{1}H NMR ($CDCl_3$, 400 MHz) spectra for the cycloaddition reaction of ECH only (Table S9, entry no. 2).

Figure S14. ^{1}H NMR ($CDCl_3$, 400 MHz) spectra for the cycloaddition reaction of ECH using TBAB only (Table S9, entry no. 3).

Figure S15. ^{1}H NMR ($CDCl_3$, 400 MHz) spectra for the cycloaddition reaction of ECH using MOF**1'** and TBAB carried out for 3h at 80°C (Table S9, entry no.4).

Figure S16. ^{1}H NMR ($CDCl_3$, 400 MHz) spectra for the cycloaddition reaction of ECH using MOF**1'** and TBAB carried out for 6h at 80°C (Table S9, entry no. 5 and table 1, entry no. 2).

Figure S17. ^{1}H NMR ($CDCl_3$, 400 MHz) spectra for the cycloaddition reaction of ECH using MOF**1'** and 0.5 mol% TBAB carried out for 9h at 80°C (Table S9, entry no. 6).

Figure S18. ^{1}H NMR ($CDCl_3$, 400 MHz) spectra for the cycloaddition reaction of ECH using MOF**1'** and 1.5 mol% TBAB carried out for 9h at 80°C (Table S9, entry no.7).

Figure S19. ^{1}H NMR ($CDCl_3$, 400 MHz) spectra for the cycloaddition reaction of ECH using MOF**1'** and TBAB carried out for 9h at 80°C (Table S9, entry no.8 and table 1, entry no. 1).

Figure S20. ^{1}H NMR ($CDCl_3$, 400 MHz) spectra for the cycloaddition reaction of epichlorohydrin using 0.1 mol% MOF**1'** and TBAB carried out for 9h at 80°C (Table S8, entry no.9).

Figure S21. ^{1}H NMR ($CDCl_3$, 400 MHz) spectra for the cycloaddition reaction of ECH using MOF**2** (Sm^{+3}) and TBAB carried out for 9 h at 80 °C (Table 1, entry no. 3).

Figure S22. ^{1}H NMR ($CDCl_3$, 400 MHz) spectra for the cycloaddition reaction of ECH using MOF**3** (Eu^{+3}) and TBAB carried out for 9 h at 80 °C (Table 1, entry no. 4).

Figure S23. ^{1}H NMR ($CDCl_3$, 400 MHz) spectra for the cycloaddition reaction of 1, 2-epoxyhexane using MOF**1'** and TBAB (Table 1, entry no.5).

Figure S24. ^{1}H NMR ($CDCl_3$, 400 MHz) spectra for the cycloaddition reaction of 1, 2-epoxydecane using MOF**1'** and TBAB (Table 1, entry no. 6).

Figure S25. ^{1}H NMR ($CDCl_3$, 400 MHz) spectra for the cycloaddition reaction of styrene oxide using MOF**1'** and TBAB (Table 1, entry no.7).

Table S10. Optimized geometries of epoxides using Gaussian09 at b3lyp/6-311g (d,p) level.

Table S11. Cycloaddition reaction of CO_2 with mixed epoxides using MOF**1'** as catalyst.

Figure S26. ^{1}H NMR ($CDCl_3$, 400 MHz) spectra for the cycloaddition reaction of mixed epoxides (ECH + 1, 2-epoxyhexane) using MOF**1'** and TBAB carried out for 9h at 80°C (Table S11, entry no. 1).

Figure S27. ^{1}H NMR ($CDCl_3$, 400 MHz) spectra for the cycloaddition reaction of mixed epoxides (ECH + 1, 2-epoxydecane) using MOF**1'** and TBAB carried out for 9h at 80°C (Table S11, entry no.2).

Figure S28. ^{1}H NMR ($CDCl_3$, 400 MHz) spectra for the 5th regeneration cycle of ECH using MOF**1'** and TBAB carried out for 9h at 80°C (Table S9, entry no. 10).

(a) Physical measurements

Powder X-ray diffraction measurements were conducted in the range of 2Theta value of 5-50° on PANanalytical's X'PERT PRO X-Ray diffractometer with a scan rate of 2°/min using Cu-Kα radiation (λ = 1.54184 Å; 40kV, 20mA) for confirming phase purity of as-synthesized samples of MOF**1-3**. Elemental analyses of the samples were carried out on ThermoFishcer Flash 2000 Elemental analyser. Thermogravimetric analyses of the as-synthesized samples were carried out using Metler Toledo thermogravimetric analyser under nitrogen atmosphere with a flow rate of 30mL/min from 25-600 °C (heating rate of 5°C per min).

(b) X-ray Crystallography

As synthesized crystals of MOF**1-3** were coated with paratone-N and then placed on top of glass fiber pip and then the goniometer is placed on diffractometer. The data collections were done at 298K. Single crystal X-ray structural data of MOF**1-3** were collected on a CMOS based Bruker D8 Venture PHOTON 100 diffractometer equipped with a INCOATEC micro-focus source with graphite monochromated Mo Kα radiation ($\lambda = 0.71073$ Å) operating at 50 kV and 30 mA. The SAINT[1] program was used for integration of diffraction profiles and absorption correction was made with SADABS program.[2] The structures were solved by SIR 92[3] and refined by full matrix least square method using SHELXL-2013[4] and WinGX system, Ver 2014.7.[5] The structures were refined using TWIN and BASF instructions of WinGX system. The non-hydrogen atoms in all the structures were located from the difference Fourier map and refined anisotropically. All the hydrogen atoms were fixed by HFIX and placed in ideal positions and included in the refinement process using riding model with isotropic thermal parameters. The potential solvent accessible area or void space was calculated using the PLATON[6] software. All the crystallographic and structure refinement data of the MOF**1-3** are summarized in Table 1. Selected bond lengths and angles are given in Table S1, S3 and S5 and selected hydrogen bond details of the MOF**1-3** are summarized in Table S2, S4 and S6 respectively. The crystallographic information file is deposited with the CCDC number 1962649-52 for MOF**1-3** respectively.

(c) Synthesis of H_2ImBDC.HCl.H_2O ligand

The synthesis of H_2ImBDC.HCl.H_2O ligand was carried out using previously reported procedure.[7] A mixture of potassium carbonate (1.934 g, 14 mmol), imidazole (1.71 g, 25 mmol), 2-brotmoterphthalic acid (1.225 g, 5 mmol) and copper sulphate pentahydrate (0.050 g, 0.2 mmol) were grinded sufficiently in pestle mortar to make a homogeneous mixture. Then, the mixture was transferred in 100 mL round bottom flask and degassed under vacuum for 30 minutes. Further, the mixture was heated at 210°C for 10 h under nitrogen atmosphere. After completion of reaction, the solid reaction mixture was allowed to cool down to room temperature. Then, it was dissolved in 60 mL of deionized water and filtered. The obtained filtrate was adjusted with 6M dilute HCl to achieve 2-3 pH value and filtered to obtain grey precipitate. Re-crystallization from dilute hydrochloric acid gives colourless needle-like crystals of H_2ImDBC.HCl.H_2O. ^1H NMR (DMSO-d_6, 25 °C): $\delta = 7.85$ (s, 1H, N-CH-CH-N), 8.04 (s, 1H, N-CH-CH-N), 8.20-8.28 (br, 3H, Ar-H), 9.50 (s, H, N-CH-N).

(d) Adsorption measurements

N_2 adsorption measurements were performed at 77 and 273K, while H_2 and Ar adsorption-desorption measurements were conducted at 273K. CO_2 adsorption-desorption measurements were conducted at 195, 273 and 298K on a Quantachrome QUADRASORB-SI automatic volumetric instrument Ultrapure (99.995%) N_2, H_2, He, Ar, and CO_2 gases were used for the adsorption-desorption measurements. Prior to adsorption measurements, the acetonitrile exchanged sample (~ 0.10 g) was activated at 373 K under vacuum (18 mTorr) for 15 hours using Flovac degasser from Quantachrome. The temperature, 77 K was maintained using liquid nitrogen as a coolant and 273 and 298 K was achieved for CO_2 uptake measurements by using a Julabo chiller with an ethylene glycol-water mixture (1:1) as a coolant. 195 K temperature was maintained using an acetone-dry ice slush bath as a coolant for CO_2 measurements. Then, the degassed MOF sample was introduced to the surface area analyzer and all the other operations were computer controlled. Further, the gas selectivity experiments were conducted at 273 K and the dead volume of the sample cell was measured using Helium gas.

(e) Analysis of gas adsorption isotherms

Clausius-Clapeyron equation[8] was used to calculate the enthalpies of hydrogen adsorption. By using Langmuir Freundlich equation[9] an accurate fit was retrieved which gives a precise prediction of hydrogen adsorbed at saturation. A modification of Clausius-Clapeyron equation is used for calculations.

$$\ln\left[\frac{P_1}{P_2}\right] = \Delta H_{ads} \; X \left[\frac{T_2 - T_1}{R \; X \; T_2 T_1}\right] \qquad \text{------(i)}$$

where, P_1 and P_2 = pressures for isotherm at 273K and 298K respectively.

T_1 and T_2 = temperatures for isotherm at 273K and 298K respectively.

ΔH_{ads} = Enthalpy of adsorption.

R = Universal gas constant = 8.314 J/K/mol.

Pressure is a function of amount of gas adsorbed which was determined by using the Langmuir-Freundlich fit.

$$\frac{Q}{Q_m} = \frac{B \; X \; P^{(1/t)}}{1 + (B \; X \; P^{(1/t)})} \qquad \text{------(ii)}$$

where, Q = moles of gas adsorbed.

Q_m = moles of gas adsorbed at saturation.

B and t = constants.

P = Pressure.

By rearranging equation (ii) we get equation (iii)

$$P = \left[\frac{Q/Q_m}{B - (B \text{ X } Q/Q_m)} \right]^t \qquad \text{------(iii)}$$

Substituting equation (iii) into equation (i) we get

$$\Delta H_{ads} = \frac{R \text{ X } T_1 \text{ X } T_2}{T_2 - T_1} \ln \frac{\left[\frac{Q/Q_{m1}}{B - (B \text{ X } Q/Q_{m1})} \right]^{t1}}{\left[\frac{Q/Q_{m2}}{B - (B \text{ X } Q/Q_{m2})} \right]^{t2}} \qquad \text{------(iv)}$$

In equation (iv), subscript 1 and 2 are representing data corresponding to 273K and 298K in case of carbon dioxide gas.

(f) Calculation of gas (CO_2/N_2) selectivity using IAST method

The gas selectivity for CO_2/N_2 (15:85) was calculated at 273 K following the ideal adsorbed solution theory (IAST) proposed by Myers and Prausnitz. The IAST theory assumes that the adsorbed phase is a two-dimensional solution in equilibrium with the gas phase. Both the components in the mixture behave as ideal adsorbed solution and conform to the rule analogous to Raoult's law. In order to calculate the selective sorption performance of MOF**1** toward the separation of binary mixed gases, the parameters fitted from the single-component CO_2 and N_2 adsorption isotherms based on the dual-site Langmuir-Freundlich equation given below is followed.

$$q = q_{sat,1} \left[\frac{k_1 c^n}{1 + k_1 c^n} \right] + q_{sat,2} \left[\frac{k_2 c^n}{1 + k_2 c^n} \right]$$

where q is the adsorbed amount (mmol/g), $q_{sat,1}$ and $q_{sat,2}$ are the saturation capacities of sites 1 and 2 (mmol/g); k_1 and k_2 are the affinity coefficients of sites 1 and 2, c is the equilibrium pressure (kPa) and 1/n1 and 1/n2 represent the deviation from an ideal homogeneous surface.

The predicted adsorption selectivity is defined as

$$S = \left[\frac{x_1/y_1}{x_2/y_2} \right]$$

Where, x_i is the mole fractions of component i in the adsorbed and y_i is the mole fractions of component i in bulk phase. The IAST calculations were carried out for a binary mixture containing 15% CO_2 (y_1) and 85% N_2 (y_2), which is a typical composition of flue gases.

(g) Catalytic cycloaddition reactions

All of the catalytic reactions were carried out with a CO_2 pressure of 0.1 MPa in a 50 mLstainless steel high-pressure reactor. Prior to catalytic reactions, the catalysts were activated at 373 K for 15 h under vacuum to remove the guest and metal-coordinated H_2O molecules and then transferred to the reactor. All of the reactants/reagents including the internalstandard were added at room temperature, the reactor was pressurized with CO_2 (up to 0.5 MPa) and flushed twice, and then the required pressure was attained (0.1 MPa) for 9 h. The reaction mixture was stirred at 800 rpm under pressurized conditions for 9 h. After catalytic reactions, the pressure was released slowly, the catalyst was separated by filtration, and the catalytic conversion was determined by ^1H NMR spectroscopy using 1,1′,2,2′-tetrachloroethane as a reference standard. The recovered catalyst after catalytic reaction was washed with methanol (MeOH) three times, dried at 373 K for 10 h under vacuum, and then reused for successive cycles.

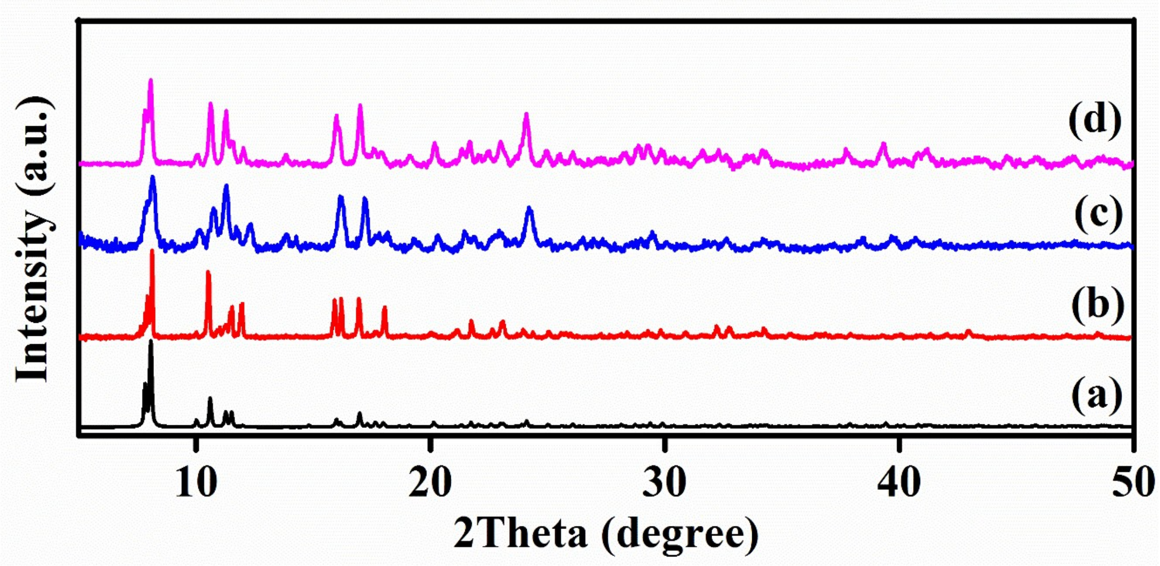

Figure S1. PXRD patterns of MOF**1**(Tb^{+3}) (a) pattern calculated from the single crystal X-ray data (b) for as-synthesized sample (c) for the sample activated at 373 K for 15 hours and (d) the sample recovered after five cycles of catalysis.

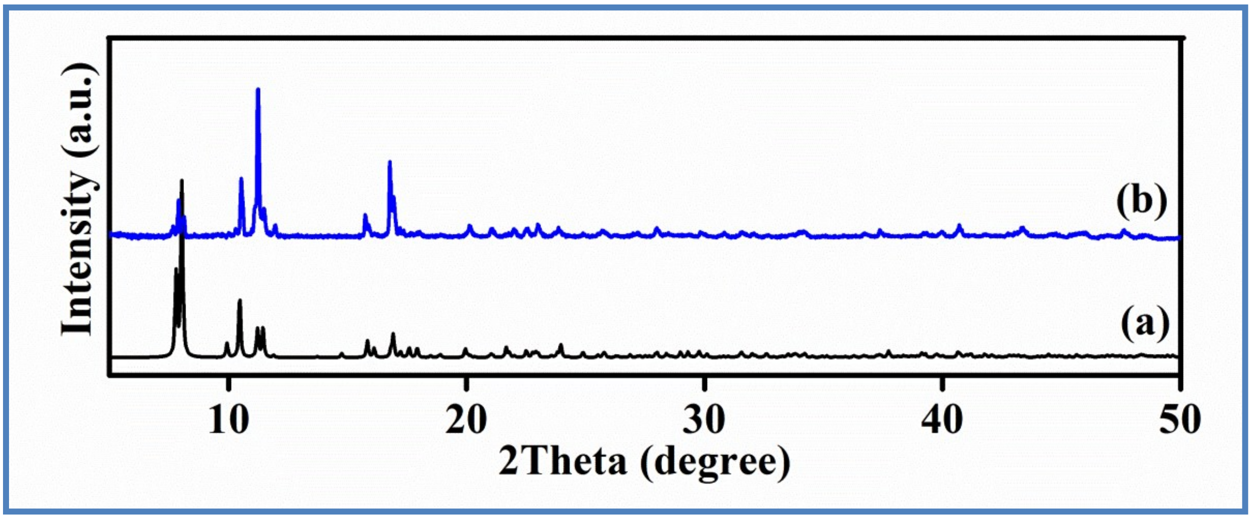

Figure S2. PXRD patterns of MOF**2** (Sm^{+3}) (a) pattern calculated from the single crystal X-ray data (b) for as-synthesized sample.

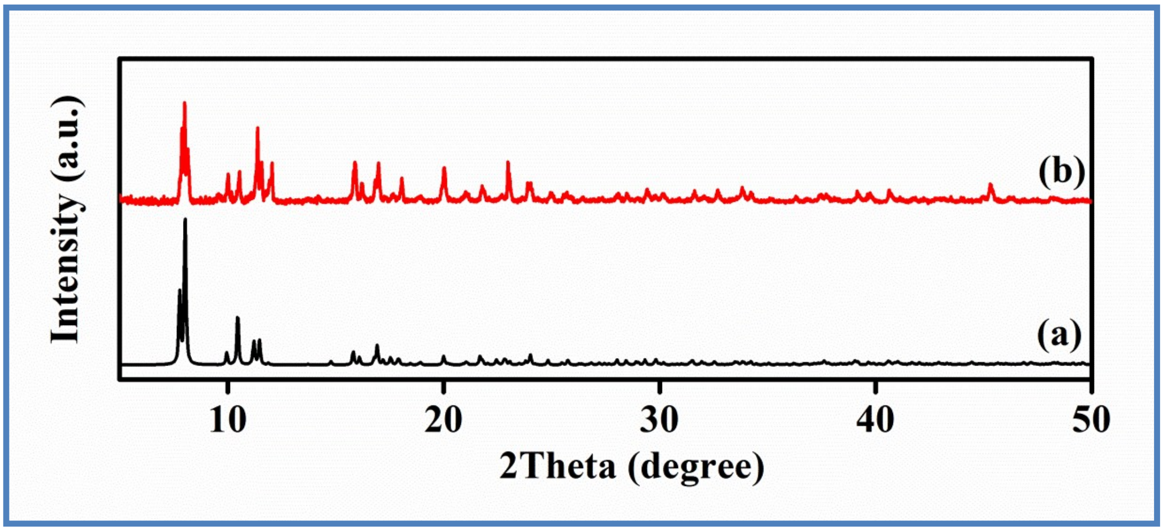

Figure S3. PXRD patterns of MOF**3** (Eu^{+3}) (a) pattern calculated from the single crystal X-ray data (b) for as-synthesized sample.

Table S1. Selected bond lengths (Å) and angles (°) for MOF**1** (Tb^{+3}).

Tb1-O1	2.611(6)	Tb2-O1	2.350(6)
Tb1-O2	2.551(7)	Tb2-O5	2.578(6)
Tb1-O3	2.3316(6)	Tb2-O6	2.455(6)
Tb1-O4	2.445(7)	Tb2-O7	2.477(4)
Tb1-O5	2.408(7)	Tb2-O8	2.352(7)
Tb1-O9	2.345(6)	Tb2-O10	2.376(7)
Tb1-O14	2.523(7)	Tb2-O11	2.555(14)
Tb1-O15	2.394(7)	Tb2-O12	2.389(13)
Tb1-N1	2.573(10)	Tb2-N6	2.446(9)
O1-Tb1-O2	51.6(2)	O1-Tb1-O3	124.7(2)
O1-Tb1-O4	71.9(2)	O1-Tb1-O5	67.43(19)
O1-Tb1-O9	70.53(18)	O1-Tb1-O14	135.2(2)
O1-Tb1-O15	145.5(2)	O1-Tb1-N1	109.5(3)
O1-Tb2-O5	68.8(2)	O1-Tb2-O6	118.5(2)
O1-Tb2-O7	126.13(17)	O1-Tb2-O8	76.4(2)
O1-Tb2-O10	89.6(3)	O1-Tb2-O11	75.8(2)
O1-Tb2-O12	76.91(18)	O1-Tb2-N6	151.1(2)
O2-Tb1-O3	79.8(2)	O2-Tb1-O4	93.8(3)
Tb1-O1-Tb2	111.8(2)	O2-Tb1-O5	118.7(2)
Tb1-O5-Tb2	111.0(2)	O2-Tb1-O9	80.4(2)
O3-Tb1-O5	142.7(2)	O3-Tb1-O9	77.7(2)
O3-Tb1-O14	74.2(2)	O3-Tb1-O15	89.4(2)
O3-Tb1-N1	72.5(2)	O4-Tb1-O5	70.4(2)
O4-Tb1-O9	135.9(2)	O4-Tb1-O14	118.2(2)
O4-Tb1-O15	76.8(3)	O4-Tb1-N1	72.4(3)
O5-Tb1-O9	74.56(19)	O5-Tb1-O14	75.4(2)
O5-Tb1-O15	88.9(2)	O5-Tb1-N1	141.5(2)
O5-Tb2-N6	114.4(5)	O5-Tb2-O6	49.7(2)
O5-Tb2-O7	107.31(18)	O5-Tb2-O8	76.0(2)
O5-Tb2-O10	149.6(2)	O5-Tb2-O11	133.9(2)
O5-Tb2-O12	70.91(19)	O6-Tb2-O7	77.4(2)

O6-Tb2-O8	89.0(2)	O6-Tb2-O10	145.6(3)
O6-Tb2-O11	147.7(2)	O6-Tb2-O12	81.9(2)
O6-Tb2-N6	72.7(3)	O7-Tb2-O8	157.2(2)
O7-Tb2-O10	102.7(2)	O7-Tb2-O11	71.3(2)
O7-Tb2-O12	53.46(17)	O7-Tb2-N6	81.2(2)
O8-Tb2-O10	78.3(3)	O8-Tb2-O11	123.2(2)
O8-Tb2-O12	143.2(2)	O8-Tb2-N6	77.3(3)
O9-Tb1-O14	76.3(2)	O9-Tb1-O15	128.6(3)
O9-Tb1-N1	142.7(2)	O10-Tb2-O11	53.2(3)
O10-Tb2-O12	126.4(2)	O10-Tb2-N6	73.3(3)
O11-Tb2-O12	73.2(2)	O11-Tb2-N6	109.6(3)
O12-Tb2-N6	132.0(2)	O14-Tb1-N1	115.2(3)
O14-Tb1-O15	52.4(3)	O15-Tb1-N1	73.4(3)

Table S2. Selected hydrogen bonding geometry (Å, °) for MOF**1** (Tb^{+3}).

D–H···A	**H···A**	**D···A**	**D–H···A**
C6-H6…O14^{i}	2.5300	2.850(14)	100.00
C7-H7...O15^{i}	2.4600	2.778(13)	100.00
C11-H11…O15	2.3900	2.903(13)	115.00
C33-H33...O11^{ii}	2.4300	3.245(10)	146.00
C35-H35...O10^{iii}	2.5700	2.969(14)	106.00

Symmetry operations: i = x, 1+y, z; ii = x, y, -1+z

Table S3. Selected bond lengths (Å) and angles (°) for MOF**2** (Sm^{+3}).

Sm1-O3	2.633(6)	Sm1-O4	2.474(7)
Sm1-O5	2.493(6)	Sm1-O6	2.544(7)
Sm1-O7	2.366(6)	Sm1-O8	2.376(7)
Sm1-O11	2.610(7)	Sm1-O15	2.433(7)
Sm1-N1	2.595(10)	Sm2-O1	2.435(6)
Sm2-O2	2.534(8)	Sm2-O3	2.363(7)
Sm2-O4	2.597(6)	Sm2-O9	2.391(7)
Sm2-O10	2.480(7)	Sm2-O12	2.519(4)
Sm2-O14	2.431(7)	Sm2-N3	2.488(9)
Sm1-O4-Sm2	110.2(2)	Sm1-O3-Sm2	112.6(2)
O1-Sm2-O2	52.4(3)	O1-Sm2-O3	89.4(2)
O1-Sm2-O4	149.7(2)	O1-Sm2-O9	78.3(2)
O1-Sm2-O10	146.2(3)	O1-Sm2-O12	103.7(2)
O1-Sm2-O14	124.8(2)	O1-Sm2-N3	73.7(3)
O2-Sm2-O3	76.8(2)	O2-Sm2-O4	135.6(2)
O2-Sm2-O9	123.1(2)	O2-Sm2-O10	147.5(2)
O2-Sm2-O12	71.29(19)	O2-Sm2-O14	72.4(2)
O2-Sm2-N3	109.1(3)	O3-Sm1-O4	67.2(2)
O3-Sm1-O5	72.5(2)	O3-Sm1-O6	136.2(2)
O3-Sm1-O7	125.00(18)	O3-Sm1-O8	70.01(19)
O3-Sm1-O11	51.3(2)	O3-Sm1-O15	146.3(2)
O3-Sm1-N1	109.3(3)	O3-Sm2-O9	76.3(3)
O3-Sm2-O10	118.2(2)	O3-Sm2-O12	125.55(19)
O3-Sm2-O14	75.8(2)	O3-Sm2-N3	150.2(2)
O3-Sm2-O4	69.4(2)	O4-Sm1-O5	69.9(2)
O4-Sm1-O7	142.3(2)	O4-Sm1-O8	74.6(2)
O4-Sm1-O11	118.3(2)	O4-Sm1-O15	90.6(2)
O4-Sm1-N1	142.3(3)	O4-Sm2-O9	75.9(2)
O4-Sm2-O10	48.9(2)	O4-Sm2-O12	106.20(16)
O4-Sm2-O14	72.04(19)	O4-Sm2-N3	114.6(3)
O5-Sm1-O6	116.8(2)	O5-Sm1-O7	145.2(2)

O5-Sm1-O8	135.8(2)	O5-Sm1-O11	94.1(2)
O5-Sm1-O15	76.2(3)	O5-Sm1-N1	73.4(3)
O6-Sm1-N1	114.4(3)	O6-Sm1-O7	73.5(2)
O6-Sm1-O8	77.9(2)	O6-Sm1-O11	149.1(2)
O6-Sm1-O15	52.2(3)	O7-Sm1-O8	77.6(2)
O7-Sm1-O11	80.7(2)	O7-Sm1-O15	88.5(5)
O7-Sm1-N1	72.3(3)	O8-Sm1-O11	80.2(2)
O8-Sm1-O15	130.1(3)	O8-Sm1-N1	141.7(3)
O9-Sm2-O10	89.2(3)	O9-Sm2-O12	157.8(2)
O9-Sm2-O14	143.2(2)	O9-Sm2-N3	76.4(3)
O10-Sm2-O12	76.9(2)	O10-Sm2-O14	83.3(2)
O10-Sm2-N3	72.9(3)	O11-Sm1-O15	144.6(3)
O11-Sm1-N1	72.1(3)	O12-Sm2-O14	53.12(19)
O12-Sm2-N3	82.9(2)	O14-Sm2-N3	133.9(3)
O15-Sm1-N1	72.5(3)		

Table S4. Selected hydrogen bonding geometry (Å, °) for MOF**2** (Sm^{+3}).

D–H···A	**H···A**	**D···A**	**D–H···A**
C1-H1…O15	2.4100	2.922(15)	115.00
C11-H11…O1	2.5900	3.016(14)	109.00
C29-H29…O1	2.4500	2.761(12)	100.00
C30-H30…O2^{i}	2.4600	3.246(10)	143.00

Symmetry operations: i = x, -1+y, z; ii = x, y, 1+z

Table S5. Selected bond lengths (Å) and angles (°) for MOF**3** (Eu^{+3}).

Eu1-O6	2.433(9)	Eu1-O7	2.350(9)
Eu1-O8	2.518(8)	Eu1-O9	2.437(8)
Eu1-O10	2.364(7)	Eu1-O12	2.595(8)
Eu1-O13	2.615(7)	Eu1-O14	2.475(8)
Eu1-N5	2.579(11)	Eu2-O1	2.433(8)
Eu2-O2	2.512(4)	Eu2-O3	2.381(8)
Eu2-O4	2.466(8)	Eu2-O5	2.556(9)
Eu2-O6	2.599(7)	Eu2-O13	2.376(8)
Eu2-O15	2.400(7)	Eu2-N1	2.497(13)
O1-Eu2-O2	53.8(2)	O1-Eu2-O3	142.8(3)
O1-Eu2-O4	82.9(3)	O1-Eu2-O5	73.0(3)
O1-Eu2-O6	71.8(3)	O1-Eu2-O13	75.9(3)
O1-Eu2-O15	125.3(3)	O1-Eu2-N1	134.3(3)
O2-Eu2-O3	157.0(3)	O2-Eu2-O4	76.7(2)
O2-Eu2-O5	72.4(2)	O2-Eu2-O6	106.9(2)
O2-Eu2-O13	126.2(2)	O2-Eu2-O15	102.8(3)
O2-Eu2-N1	83.3(3)	O3-Eu2-O4	88.8(3)
O3-Eu2-O5	122.9(3)	O3-Eu2-O6	75.2(3)
O3-Eu2-O13	76.4(3)	O3-Eu2-O15	79.1(3)
O3-Eu2-N1	75.2(4)	O4-Eu2-O5	148.2(3)
O4-Eu2-O6	49.5(3)	O4-Eu2-O13	118.1(3)
O4-Eu2-O15	145.4(3)	O4-Eu2-N1	71.6(3)
O5-Eu2-O6	135.0(3)	O5-Eu2-O13	76.2(3)
O5-Eu2-O15	52.3(3)	O5-Eu2-N1	111.4(3)
O6-Eu1-O7	74.9(3)	O6-Eu1-O8	76.4(3)
O6-Eu1-O9	89.8(3)	O6-Eu1-O10	141.8(3)
O6-Eu1-O12	118.6(3)	O6-Eu1-O13	67.6(2)
O6-Eu1-O14	69.7(3)	O6-Eu1-N5	142.7(3)
O6-Eu2-O13	68.7(3)	O6-Eu2-O15	150.1(3)
O6-Eu2-N1	113.2(3)	O7-Eu1-O8	77.1(3)
O7-Eu1-O9	129.7(3)	O7-Eu1-O10	76.3(3)

O7-Eu1-O12	80.4(3)	O7-Eu1-O13	70.7(2)
O7-Eu1-O14	136.5(3)	O7-Eu1-N5	141.4(3)
O8-Eu1-O9	52.6(3)	O8-Eu1-N5	113.5(3)
O8-Eu1-O10	73.0(3)	O8-Eu1-O12	148.3(3)
O8-Eu1-O13	136.5(3)	O8-Eu1-O14	116.9(3)
O9-Eu1-O10	89.6(3)	O9-Eu1-O12	145.1(3)
O9-Eu1-O13	145.7(3)	O9-Eu1-O14	75.3(3)
O9-Eu1-N5	72.3(3)	O10-Eu1-O12	80.3(3)
O10-Eu1-O13	124.3(2)	O10-Eu1-O14	146.0(3)
O10-Eu1-N5	72.3(3)	O12-Eu1-O13	51.2(3)
O12-Eu1-O14	94.8(3)	O12-Eu1-N5	72.7(3)
O13-Eu1-O14	72.8(3)	O13-Eu2-O15	90.6(3)
O13-Eu1-N5	110.0(3)	O13-Eu2-N1	149.7(3)
O14-Eu1-N5	74.1(3)	O15-Eu2-N1	74.0(4)

Table S6. Selected hydrogen bonding geometry (Å, °) for MOF**3** (Eu^{+3}).

D–H···A	**H···A**	**D···A**	**D–H···A**
C1-H1…O15	2.5900	2.994(16)	108.00
C6-H6…O8^{i}	2.5200	2.829(16)	100.00
C19-H19…O7^{ii}	2.4200	2.734(12)	100.00
C35-H35…O5	2.4700	3.272(12)	144.00
C36-H36…O9	2.3800	2.920(18)	116.00

Symmetry operations: i = x, 1+y, z; ii = x, y, 1+z

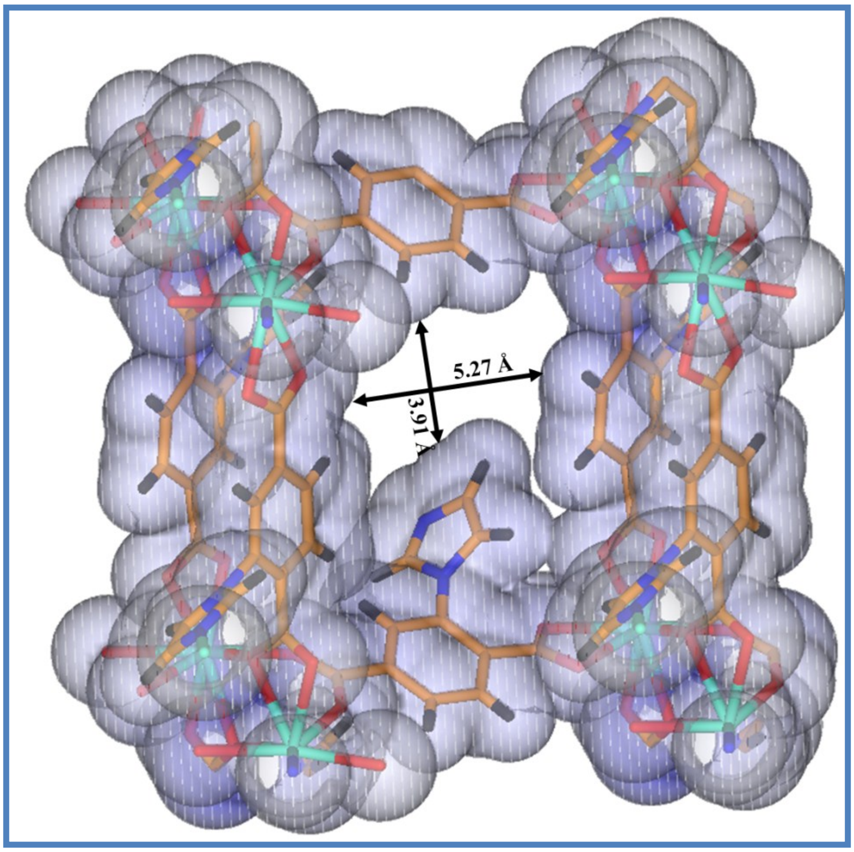

Figure S4. Pore pictures of MOF**1** (Tb^{+3}) showing pore size of 1D channels before and after interpenetration.

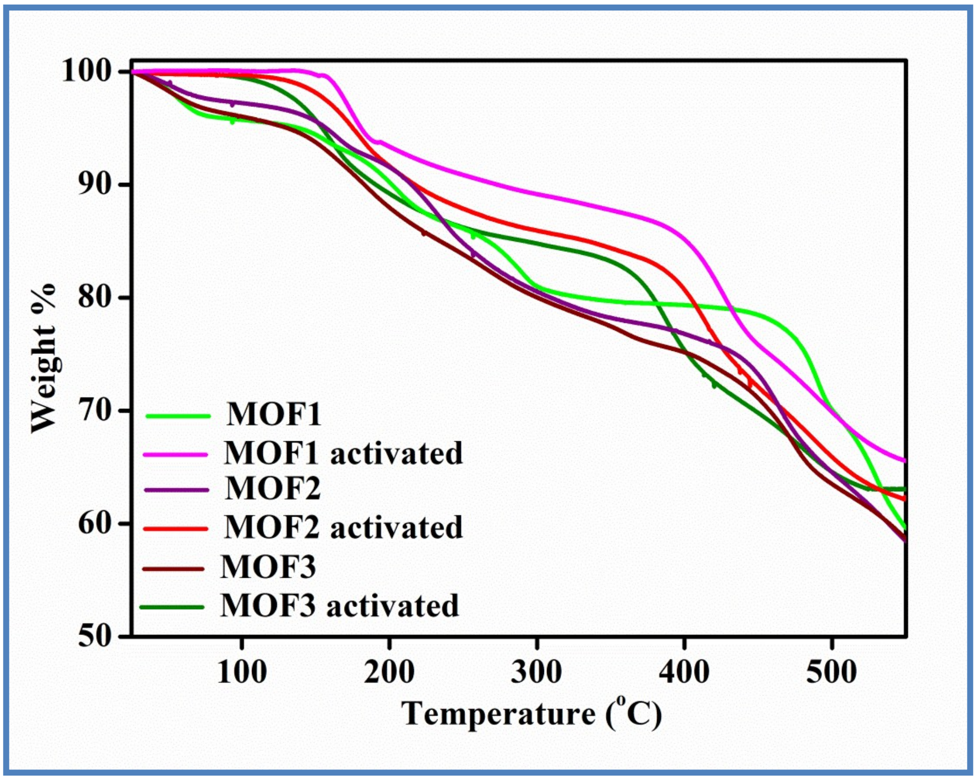

Figure S5. Thermogravimetric plots of as-synthesized and activated MOF**1-3**.

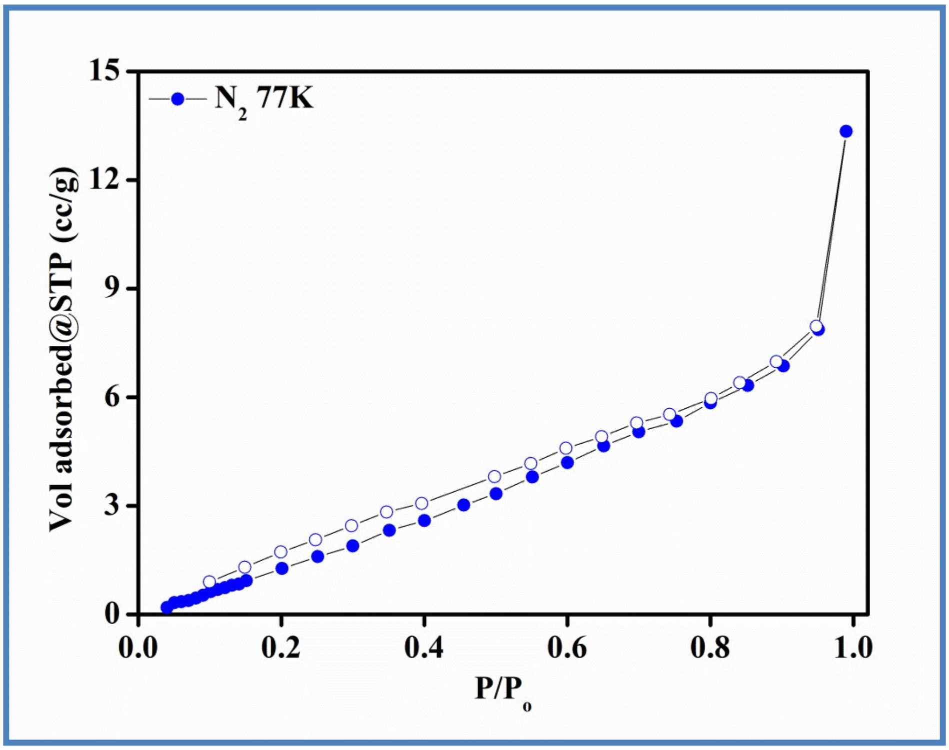

Figure S6. N_2 adsorption-desorption isotherms of MOF**1** (Tb^{+3}) carried out at 77K.

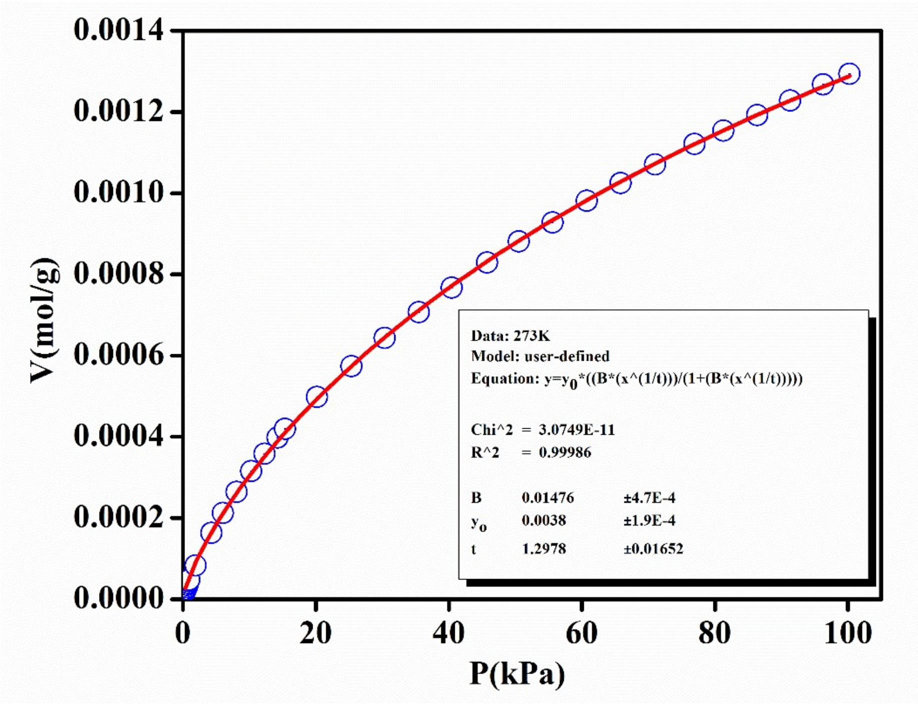

Figure S7. CO_2 adsorption isotherm for MOF**1** (Tb^{+3}) at 273 K (the solid line shows the best fit to the data using Langmuir- Freundlich equation).

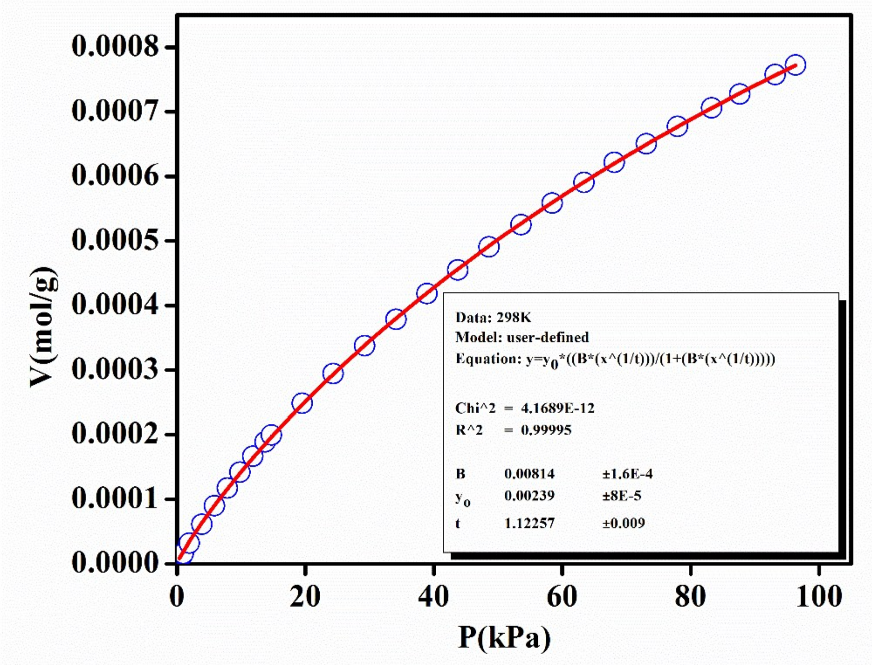

Figure S8. CO_2 adsorption isotherm for MOF**1**(Tb^{+3}) at 298 K (the solid line shows the best fit to the data using Langmuir-Freundlich equation).

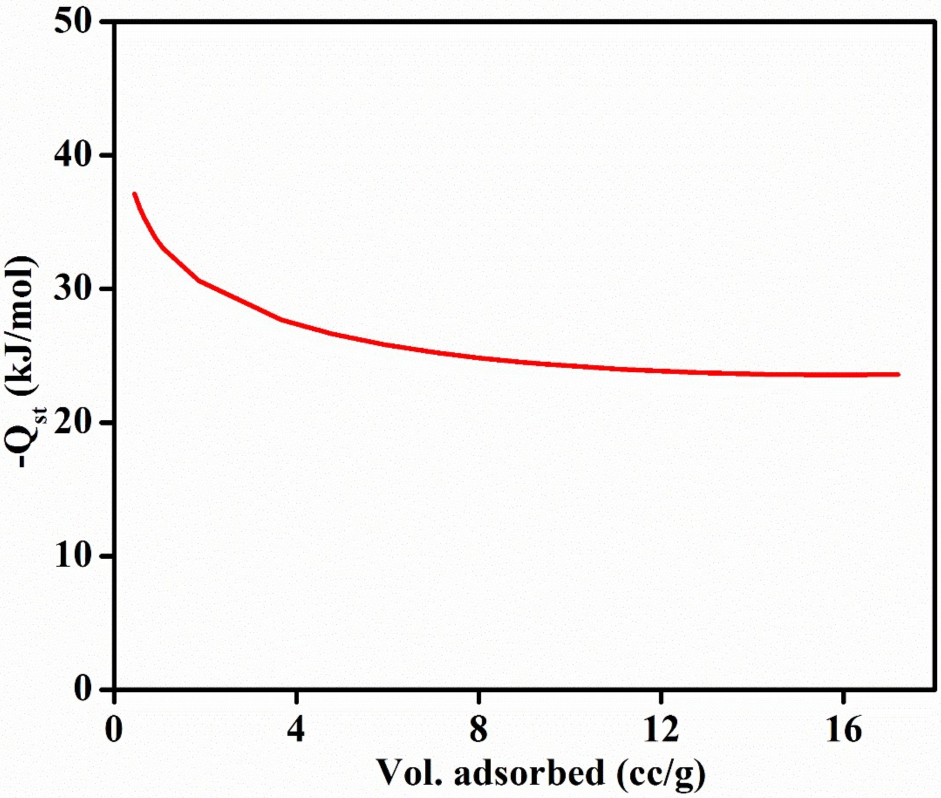

Figure S9. Enthalpy of CO_2 adsorption for MOF**1** (Tb^{+3}) calculated using Clausius-Clapeyron equation.

Table S7. Isosteric heat of adsorption (Q_{st}) values of CO_2 reported for various known lanthanides MOFs.

S. No.	**MOF**	**Q_{st} (kJ mol^{-1})**	**Ref.**
1.	$[Eu(H_2BIPA\text{-}TC)(BIPA\text{-}TC)_{0.5}\cdot 8H_2O][NH_2(CH_3)_2]$ $[Tb(H_2BIPA\text{-}TC)(BIPA\text{-}TC)_{0.5}\cdot 6H_2O][NH_2(CH_3)_2]$	23 22	10
2.	$[\{Sm(BTB)(H_2O)\}\cdot H_2O]_n$ $[\{Gd(BTB)(H_2O)\}\cdot H_2O]_n$	21.6 24.5	11
3.	$[TbL(H_2O)_2]\cdot H_2O$	~30	12
4.	$[Tb_2(ImBDC)_3.2H_2O]_n$ (**MOF1**)	37.1	**This work**
5.	**NKMOF-3-Ln** $Ln_2(INO)_4(NO_3)_2$ (Ln = La, Nd, Eu, Dy, Lu)	41 to 58	13

where, BIPA-TC = benzoimidephenanthrolinetetracarboxylic acid, BTB = 1,3,5-tris (4-carboxy phenyl) benzene), L = 1-(4-carboxybenzyl)-1H-pyrazole-3,5-dicarboxylic acid, ImBDC = 2-(imidazol-1-yl)terephthalic acid), HINO = isonicotinic acid N-oxide.

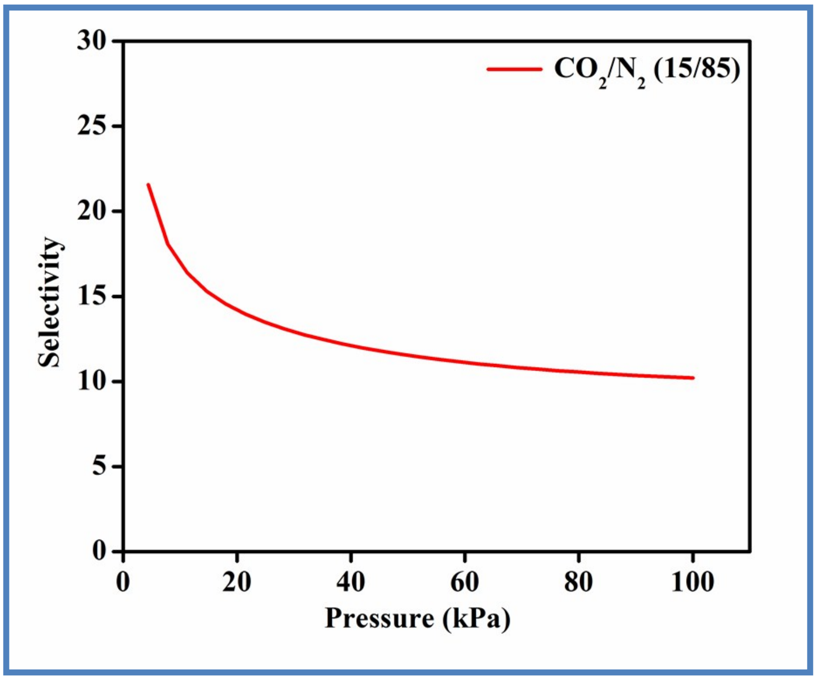

Figure S10. Binary mixture adsorption isotherms and selectivity for CO$_2$/N$_2$ (15/85) mixtures at 273 K and 1 bar pressure obtained from IAST.

Table S8. Summary of parameters for DSLF isotherm fits.

Parameters	**q_1**	**q_2**	**k_1**	**k_2**	**n_1**	**n_2**
N$_2$	0.97707	0.0458	0.00558	0.08465	1.41075	1.52774
CO$_2$	4.32018	0.12943	0.0029	0.19254	0.79966	1.56741

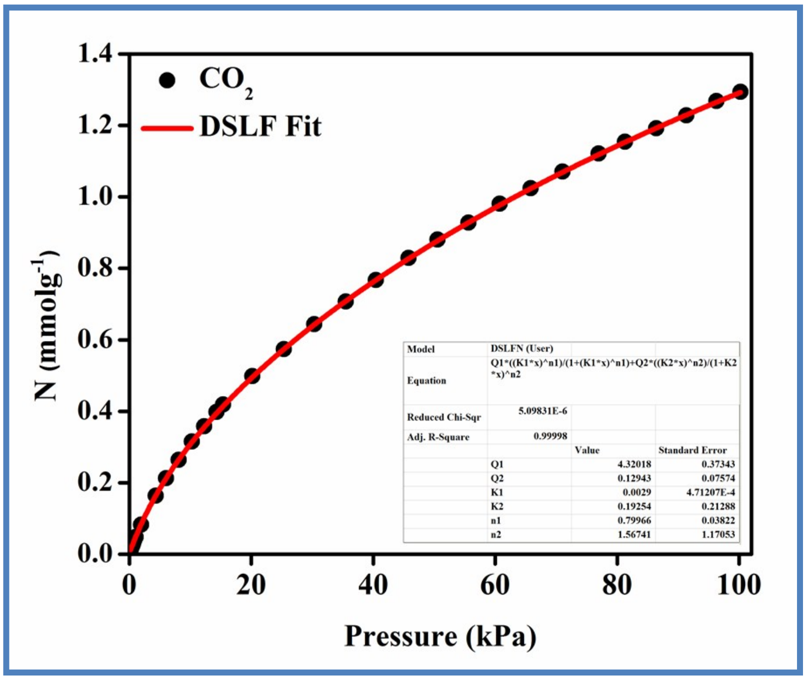

Model	DSLFN (User)		
Equation	Q1*((K1*x)^n1)/(1+(K1*x)^n1)+Q2*((K2*x)^n2)/(1+K2*x)^n2		
Reduced Chi-Sqr	5.09831E-6		
Adj. R-Square	0.99998		
		Value	Standard Error
	Q1	4.32018	0.37343
	Q2	0.12943	0.07574
	K1	0.0029	4.71207E-4
	K2	0.19254	0.21288
	n1	0.79966	0.03822
	n2	1.56741	1.17053

Figure S11. Dual site Langmuir-Freundlich fitting (red line) for CO_2 adsorption isotherms collected at 273 K and up to 1 bar pressure.

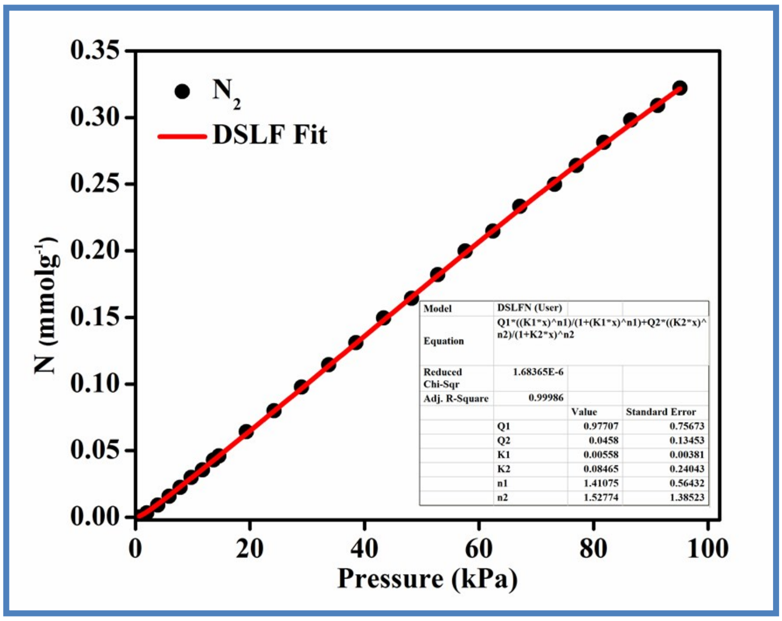

Model	DSLFN (User)		
Equation	Q1*((K1*x)^n1)/(1+(K1*x)^n1)+Q2*((K2*x)^n2)/(1+K2*x)^n2		
Reduced Chi-Sqr	1.68365E-6		
Adj. R-Square	0.99986		
		Value	Standard Error
	Q1	0.97707	0.75673
	Q2	0.0458	0.13453
	K1	0.00558	0.00381
	K2	0.08465	0.24043
	n1	1.41075	0.56432
	n2	1.52774	1.38523

Figure S12. Dual site Langmuir-Freundlich fitting (red line) for N_2 adsorption isotherms collected at 273 K and up to 1 bar pressure.

Table S9. Optimization ofcycloaddition of CO_2 with epoxides catalysed by MOF**1'**(Tb^{+3}).

Entry no.	**Catalyst (mol%)**	**Co-catalyst (mol%)**	**Pressure (MPa)**	**Time (h)**	**Temperature (^oC)**	**Conversion (%)[a]**
1.	none	none	0.1	09	r.t.	0.0
2.	none	none	0.1	09	80	0.0
3.	none	2.5	0.1	09	80	52.6
4.	0.2	2.5	0.1	03	80	35.2
5.	0.2	2.5	0.1	06	80	52.6
6.	0.2	0.5	0.1	09	80	34.3
7.	0.2	1.5	0.1	09	80	54.2
8.	0.2	2.5	0.1	09	80	>99
9.	0.1	2.5	0.1	09	80	70.2
10.[b]	0.2	2.5	0.1	09	80	95.2

[a] Conversion: the catalytic conversions were determined by ^1H NMR analysis using 1,1′,2,2′-tetrachloroethane as the internal standard. [b] Conversion for 5th regeneration cycle.

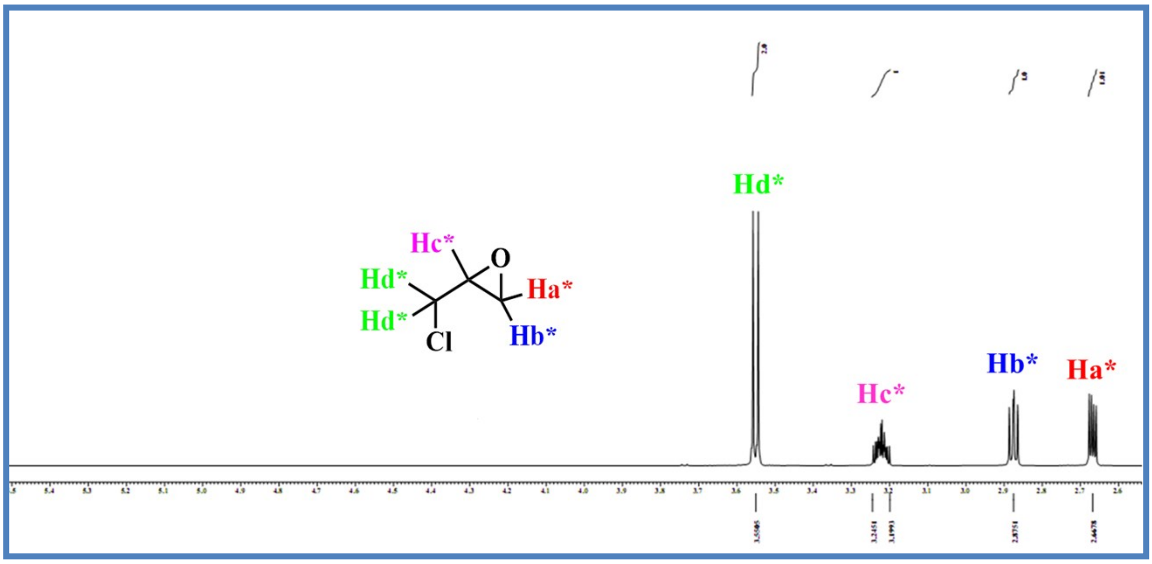

Figure S13. ^{1}H NMR ($CDCl_3$, 400 MHz) spectra for the cycloaddition reaction of ECH only (Table S9, entry no. 2).

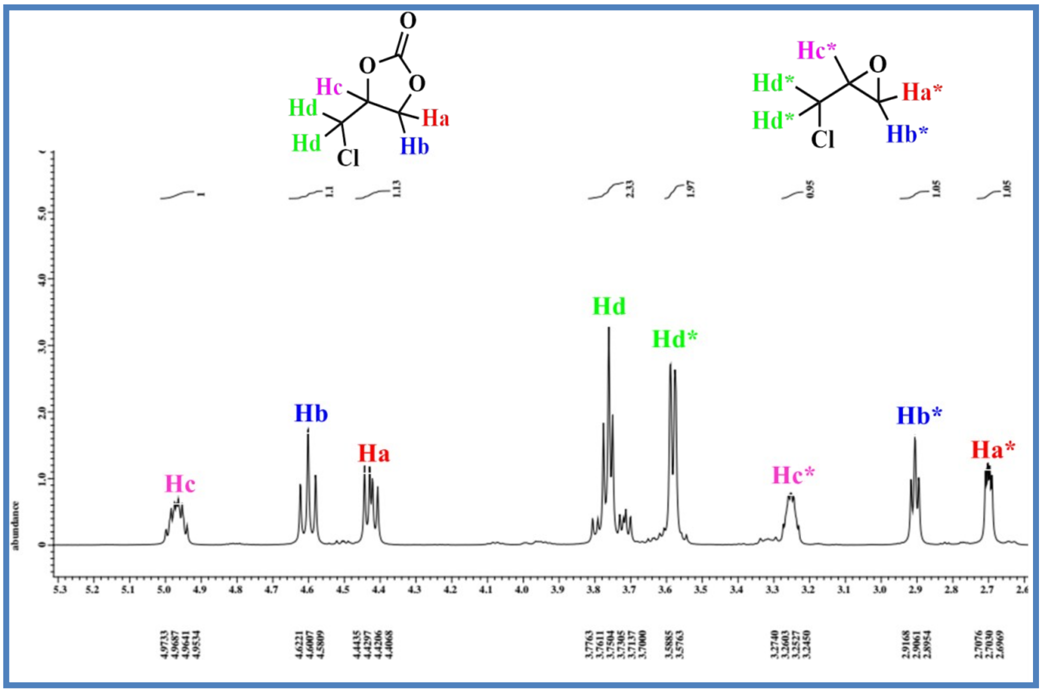

Figure S14. ^{1}H NMR ($CDCl_3$, 400 MHz) spectra for the cycloaddition reaction of ECH using TBAB only (Table S9, entry no. 3).

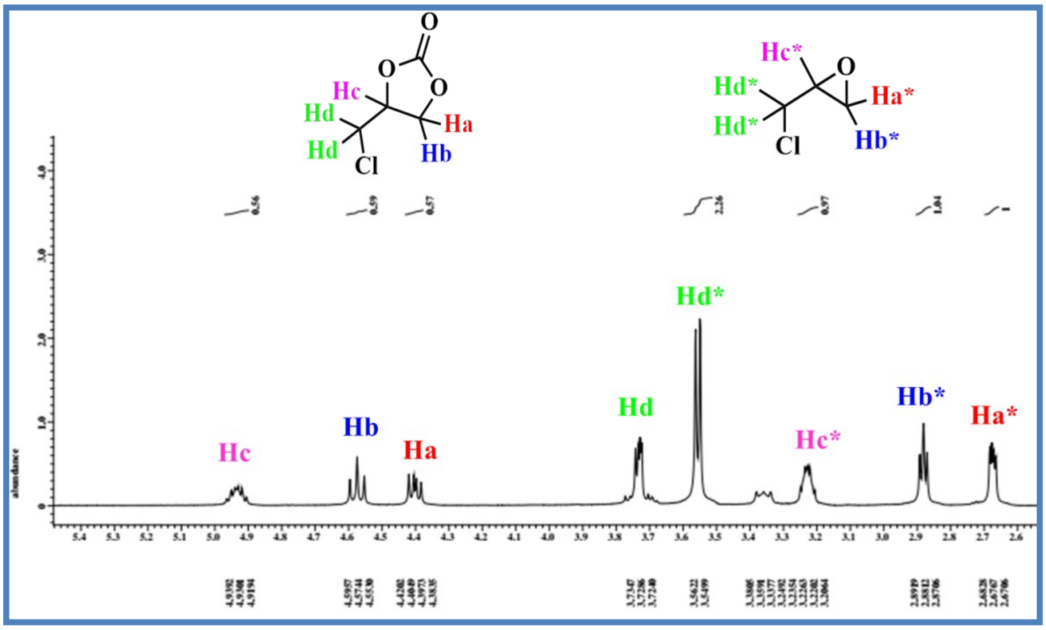

Figure S15. ^{1}H NMR ($CDCl_3$, 400 MHz) spectra for the cycloaddition reaction of ECH using MOF**1'** and TBAB carried out for 3h at 80°C (Table S9, entry no. 4).

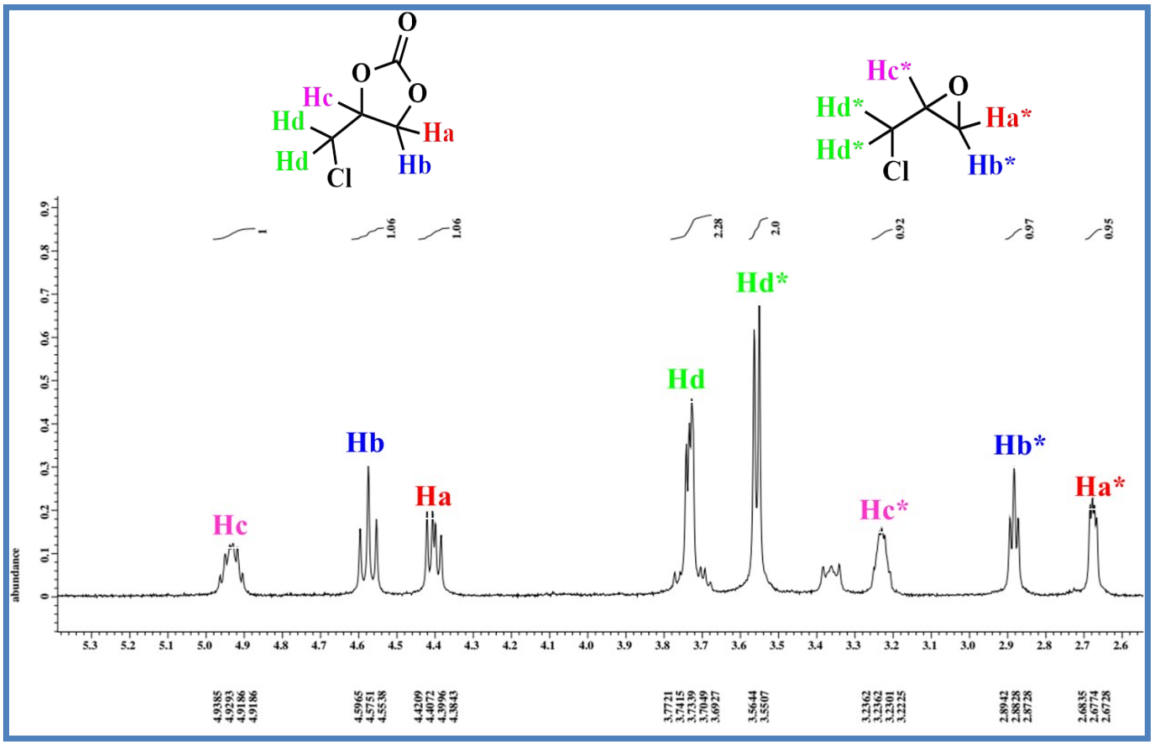

Figure S16. ^{1}H NMR ($CDCl_3$, 400 MHz) spectra for the cycloaddition reaction of ECH using MOF**1'** and TBAB carried out for 6h at 80°C (Table S9, entry no. 5 and table 1, entry 2).

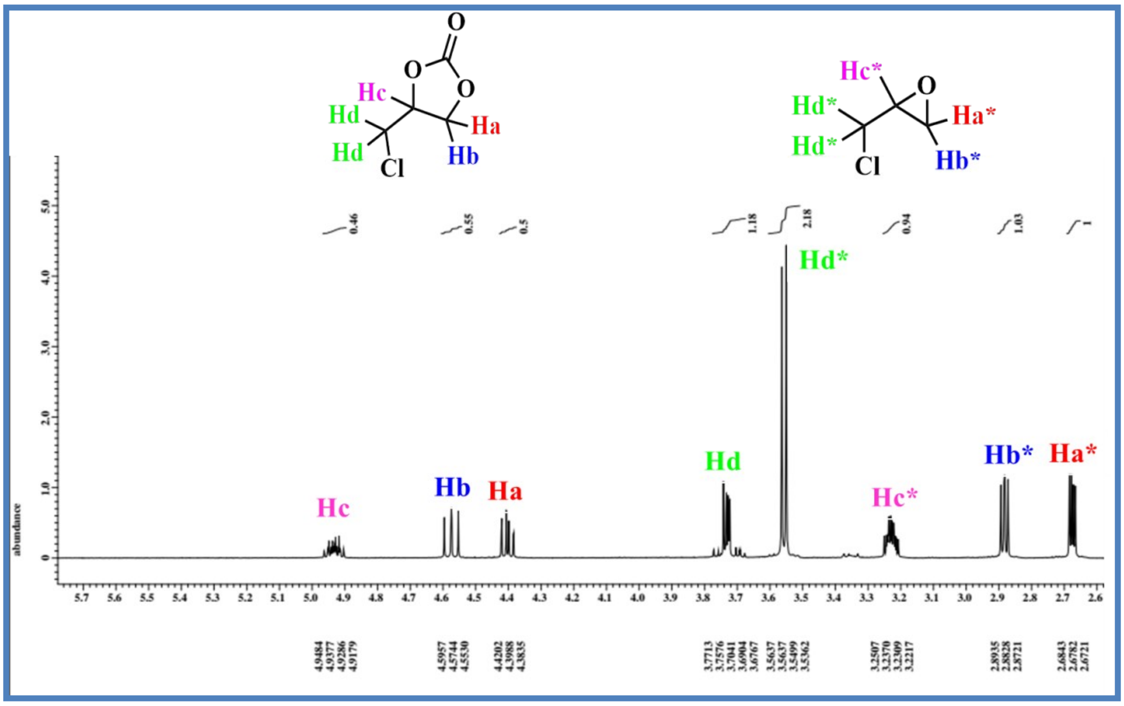

Figure S17. ^{1}H NMR ($CDCl_3$, 400 MHz) spectra for the cycloaddition reaction of ECH using MOF**1'** and 0.5 mol% TBAB carried out for 9h at 80°C (Table S9, entry no. 6).

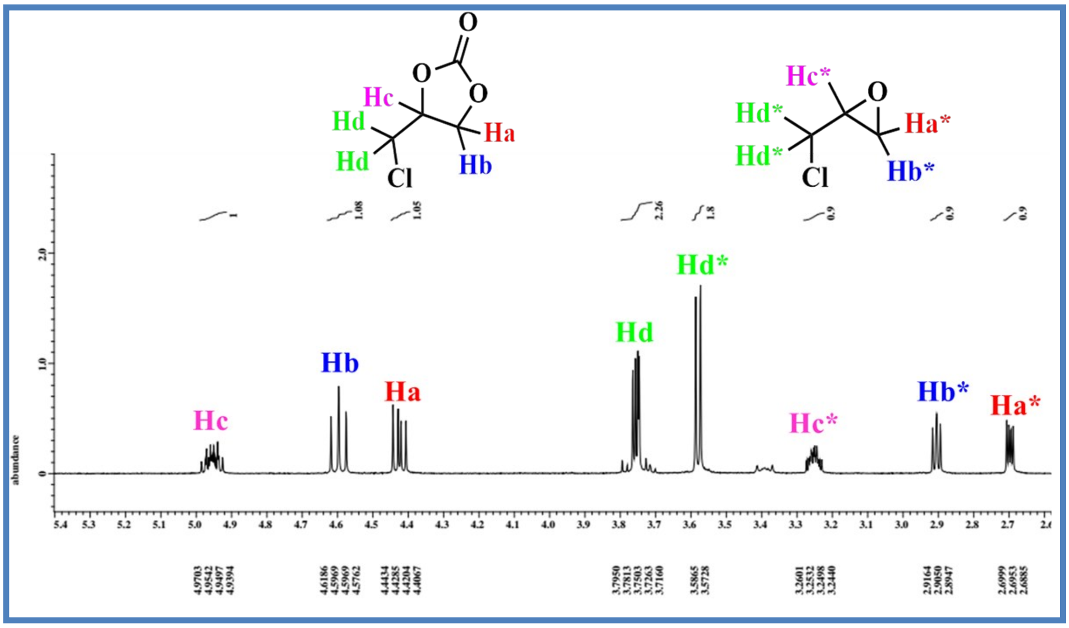

Figure S18. ^{1}H NMR ($CDCl_3$, 400 MHz) spectra for the cycloaddition reaction of ECH using MOF**1'** and 1.5 mol% TBAB carried out for 9h at 80°C (Table S9, entry no.7).

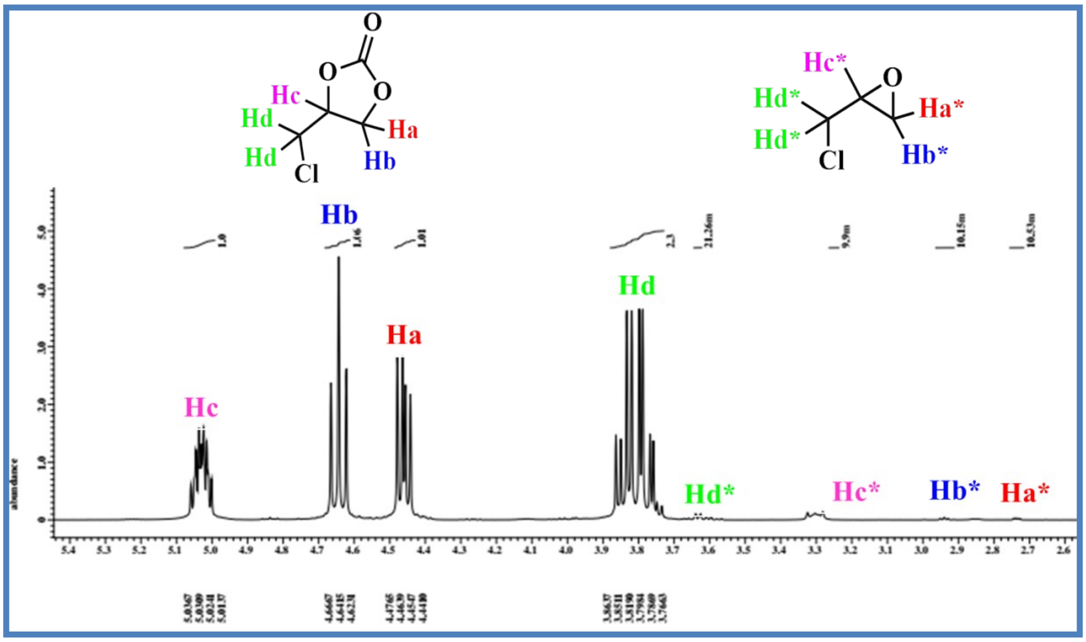

Figure S19. ^{1}H NMR ($CDCl_3$, 400 MHz) spectra for the cycloaddition reaction of ECH using MOF**1'** and TBAB carried out for 9h at 80°C (Table S9, entry no.8 and table 1, entry no. 1).

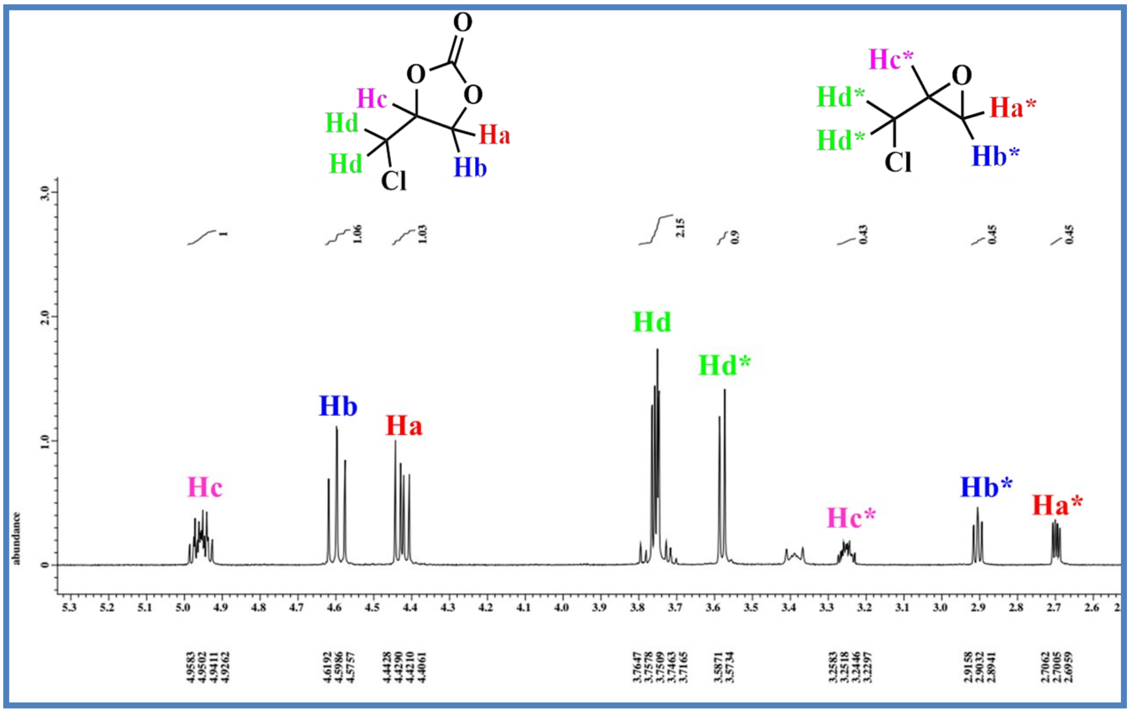

Figure S20. ^{1}H NMR ($CDCl_3$, 400 MHz) spectra for the cycloaddition reaction of ECH using 0.1 mol% MOF**1'** and TBAB carried out for 9h at 80°C (Table S9, entry no.9).

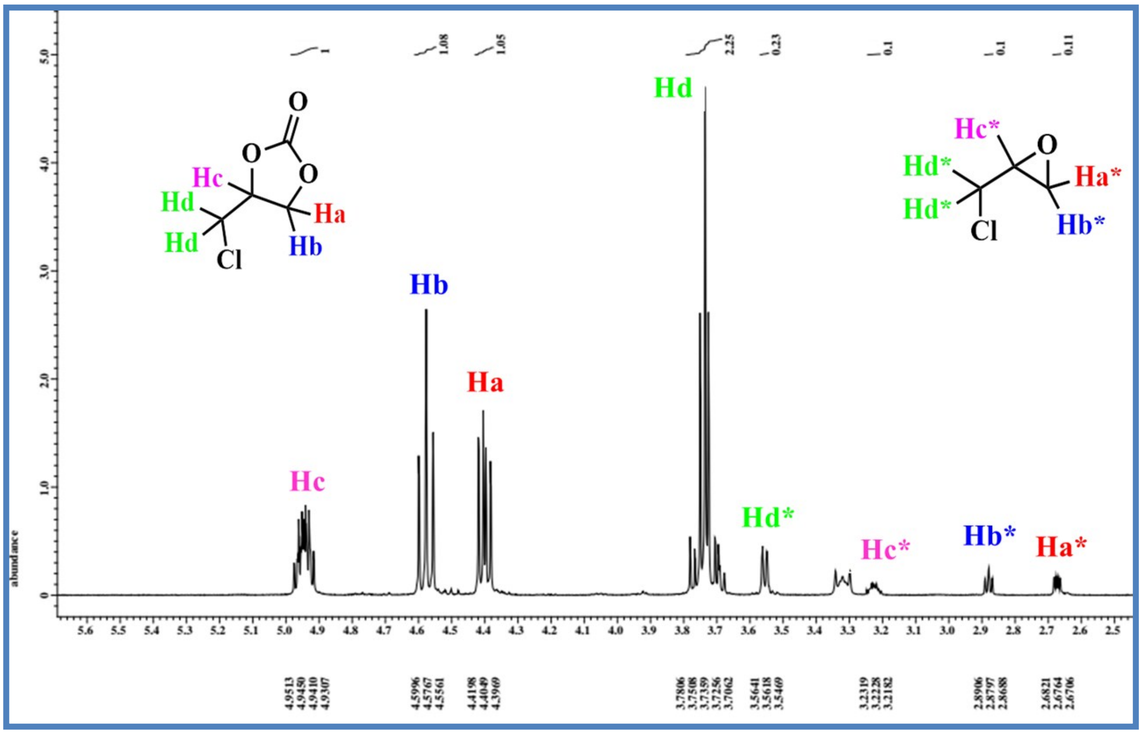

Figure S21. ^{1}H NMR ($CDCl_3$, 400 MHz) spectra for the cycloaddition reaction of ECH using MOF**2** (Sm^{+3}) and TBAB carried out for 9 h at 80 °C (Table 1, entry no. 3).

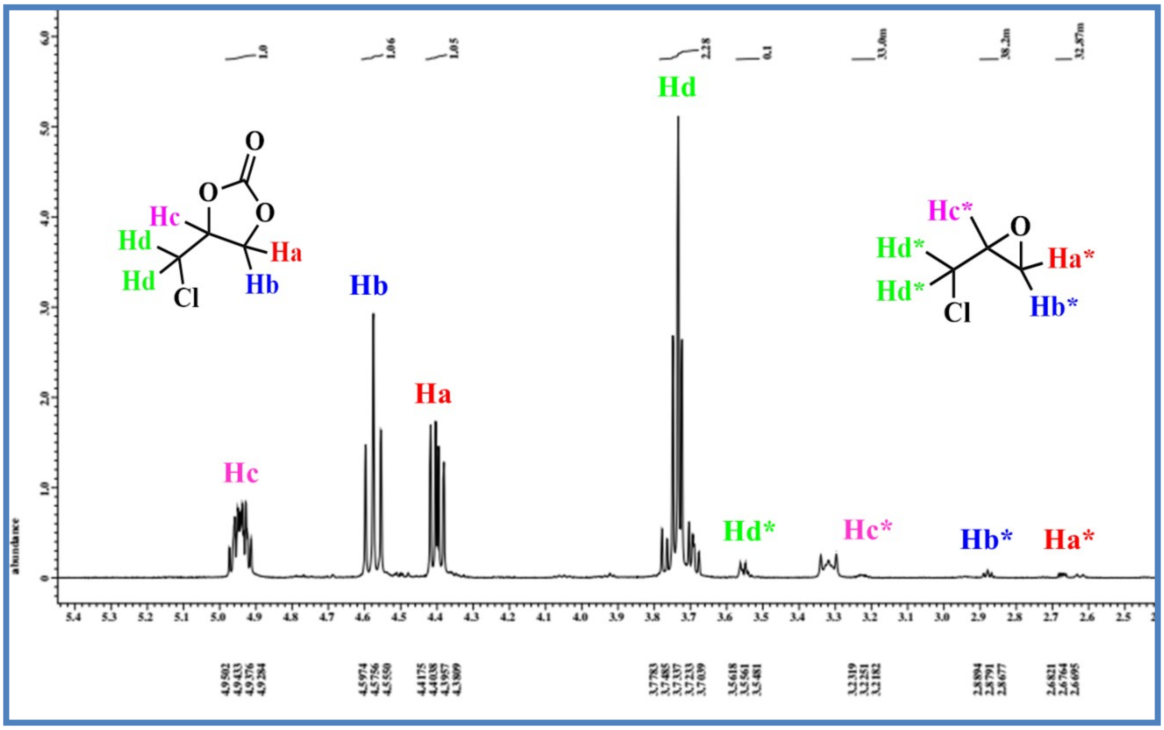

Figure S22. ^{1}H NMR ($CDCl_3$, 400 MHz) spectra for the cycloaddition reaction of ECH using MOF**3** (Eu^{+3}) and TBAB carried out for 9 h at 80 °C (Table 1, entry no. 4).

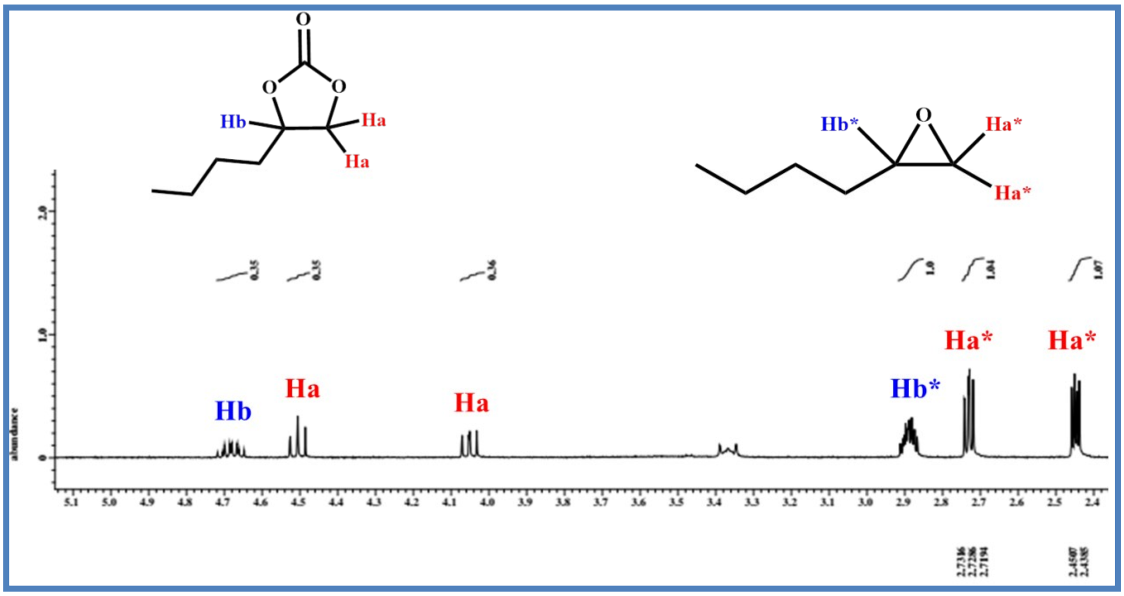

Figure S23. ^{1}H NMR ($CDCl_3$, 400 MHz) spectra for the cycloaddition reaction of 1,2-epoxyhexane using MOF**1'** and TBAB (Table 1, entry no. 5).

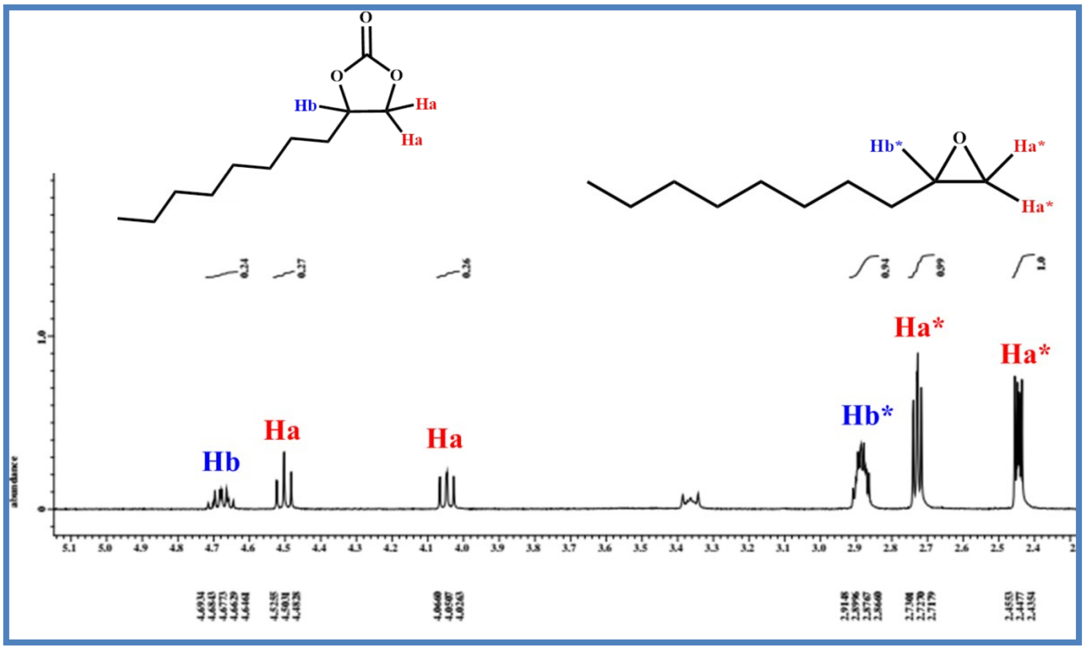

Figure S24. ^{1}H NMR ($CDCl_3$, 400 MHz) spectra for the cycloaddition reaction of 1,2-epoxydecane using MOF**1'** and TBAB (Table 1, entry no. 6).

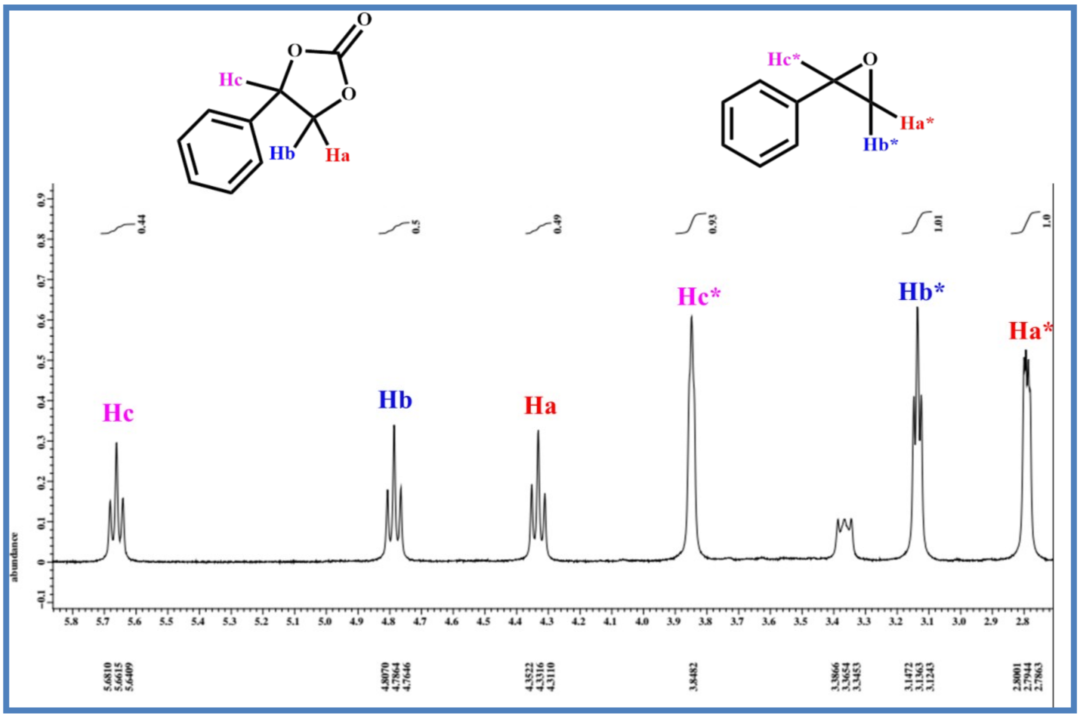

Figure S25. ^{1}H NMR ($CDCl_3$, 400 MHz) spectra for the cycloaddition reaction of styrene oxide using MOF**1'** and TBAB (Table 1, entry no.7)

Table S10. Optimized geometries of epoxides using Gaussian09[14] at b3lyp/6-311g (d,p) level.

Substrates	**Optimized structure**	**Dimensions**
Epichlorohydrin	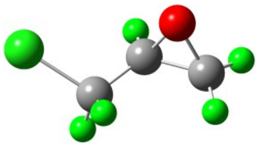	4.53 X 3.44 Å^2
1,2-epoxy hexane	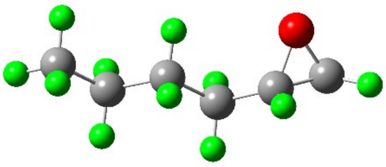	8.198 X 3.39 Å^2
1,2-epoxy decane	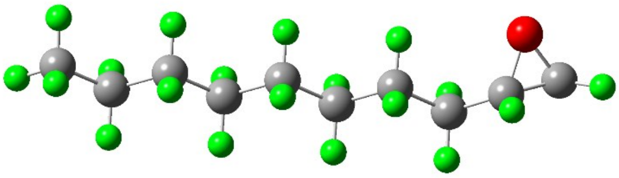	13.321 X 3.39 Å^2
Styrene oxide	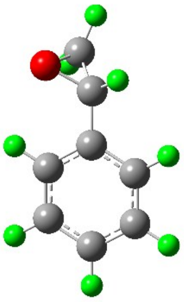	4.28 X 7.267 Å^2

Table S11. Cycloaddition reaction of CO_2 with mixed epoxides using MOF**1'** as catalyst.

S. No.	Substrate	Product	Conversion(%)
1.	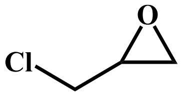 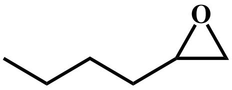	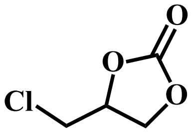 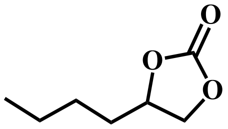	>99 6.4
2.	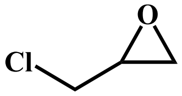 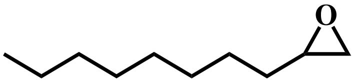	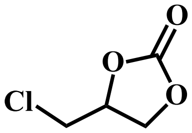 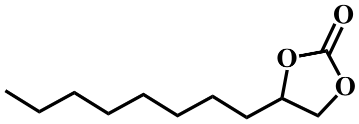	>99 3.8

[a]Conversion: the conversions were calculated by ^{1}H NMR analysis. [b]Reaction conditions: epoxides (10 mmol), catalyst/TBAB (0.2:2.5 mol%), temperature of 80 °C. Equal proportion mixed epoxides (1:1) were added.

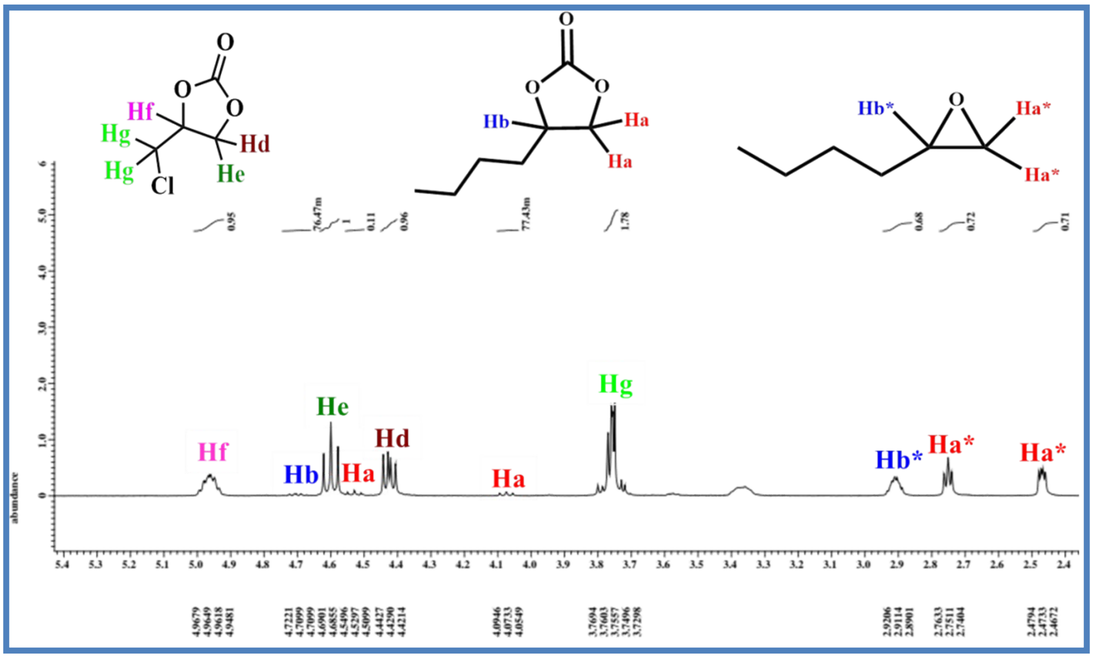

Figure S26. ^{1}H NMR ($CDCl_3$, 400 MHz) spectra for the cycloaddition reaction of mixed epoxides (ECH + 1,2-epoxyhexane) using MOF**1'** and TBAB carried out for 9h at 80°C (Table S11, entry no. 1).

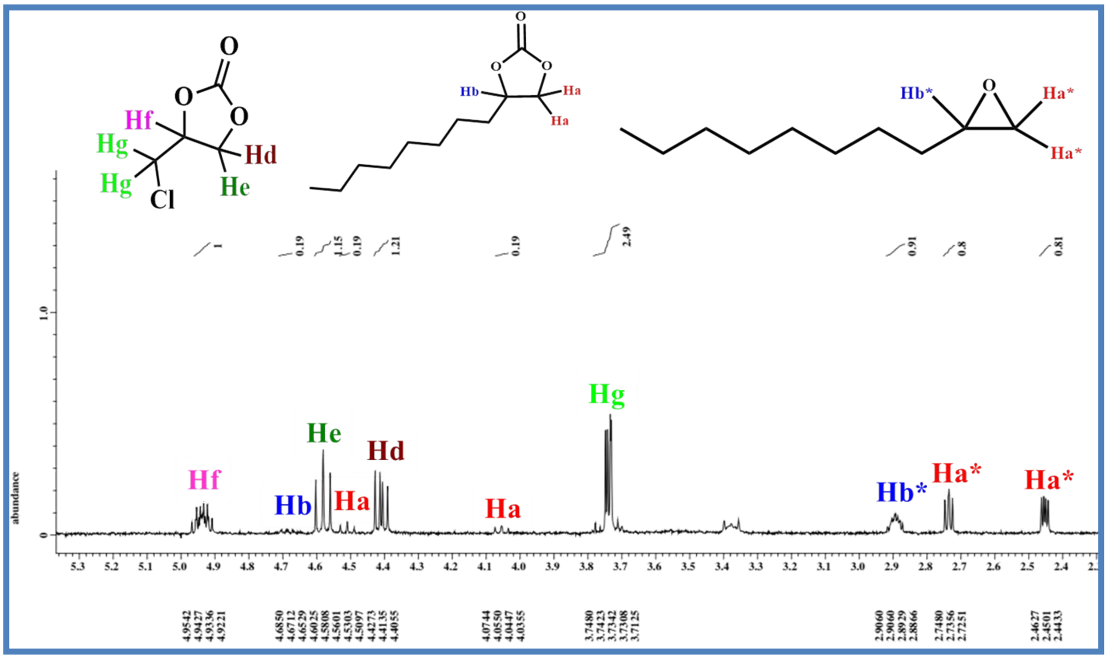

Figure S27. ^{1}H NMR ($CDCl_3$, 400 MHz) spectra for the cycloaddition reaction of mixed epoxides (ECH + 1,2-epoxydecane) using MOF**1'** and TBAB carried out for 9h at 80°C (Table S11, entry no. 2).

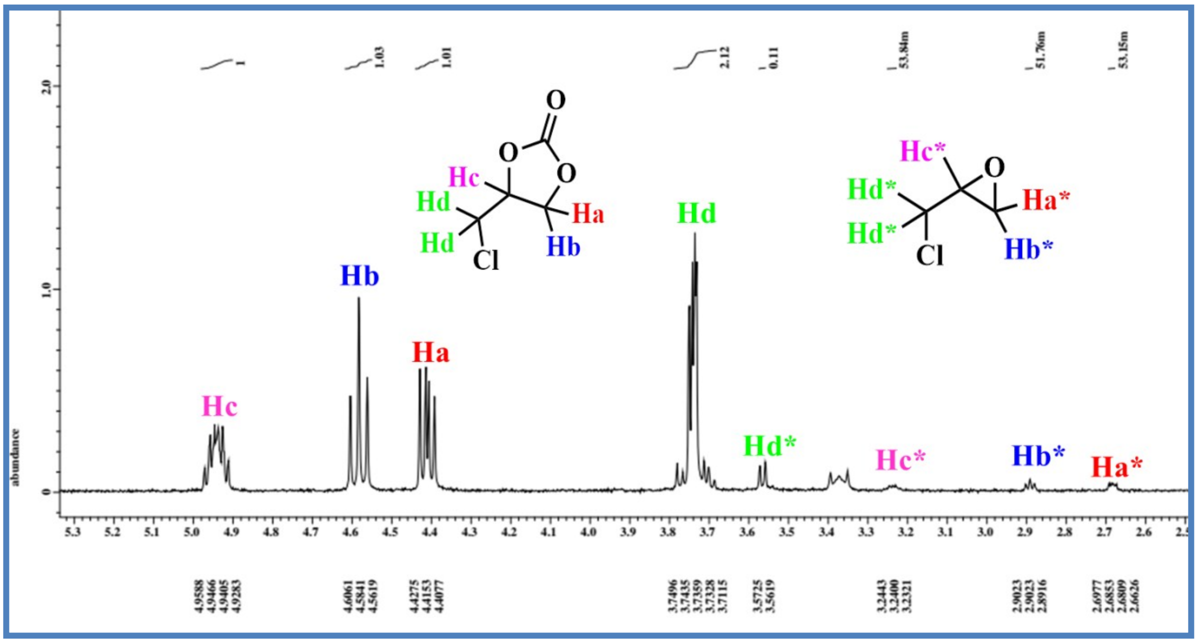

Figure S28. ^{1}H NMR (CDCl$_3$, 400 MHz) spectra for the 5th regeneration cycle of ECH using MOF**1'** and TBAB carried out for 9h at 80°C (Table S9, entry no. 10).

References

---

(1). *SMART (V 5.628), SAINT (V 6.45a), XPREP, SHELXTL*; Bruker AXS Inc., Madison, Wisconsin, USA, 2004.

(2). G. M. Sheldrick, *Siemens Area Detector Absorption Correction Program*, University of Göttingen, Göttingen, Germany, 2004.

(3). A. Altomare, G. Cascarano, C. Giacovazzo and A. Guagliardi, *J. Appl. Cryst*., 1993, **26**, 343-350.

(4). G. M. Sheldrick, SHELXL-2014, *Program for Crystal Structure Solution and Refinement*; University of Göttingen, Göttingen,Germany, 2014.

(5). L. J. Farrugia, WinGX-A Windows Programfor Crystal Structure Analysis, *J. Appl. Cryst*., 2012, **45**, 849-854.

(6). A. L. Spek, Single-crystal structure validation with the program PLATON. *J. Appl.*

Crystallogr., 2003, **36**, 7-13.

(7). J. Liang, R.-P. Chen, X.-Y. Wang, T.-T. Liu, X.-S. Wang, Y.-B. Huang and R. Cao, *Chem. Sci.*, 2017, **8**, 1570-1575.

(8). H. Pan, J. A. Ritter and P. B. Balbuena, *Langmuir*,1998, **14**, 6323-6327.

(9). (a) R. T. Yang, Gas Separation by Adsorption Processes, Butterworth, Boston, **1997**; (b) B. Ugale, S. S. Dhankhar and C. M. Nagaraja, *Cryst. Growth Des.*, 2017, **17**, 3295-3305; (c) S. S. Dhankhar and C. M. Nagaraja, *RSC Adv.*,2016, **6**, 86468-86476; (d) N. Sikdar, A. Hazra and T. K. Maji, *Inorg. Chem.*,2014, **53**, 5993-6002.

(10). H. T. D. Nguyen, Y. B. N. Tran, H. N. Nguyen, T. C. Nguyen, F. Gandara and P. T. K. Nguyen, *Inorg.Chem.*, 2018, **57**, 13772-13782.

(11). B. Ugale, S. S. Dhankhar and C. M. Nagaraja, *Cryst. Growth Des.*, 2018, **18**, 2432-2440.

(12). L. Han, T. Pham, M. Zhu, K. A. Forrest, S. Suepaul, B. Space, M. J. Zaworotko, W. Shi, Y. Chen, P. Cheng andZ. Zhang, *ACS Appl. Mater. Interfaces*, 2019, **11**, 23192-23197.

(13). T. Jing, L. Chen, F. Jiang, Y. Yang, K. Zhou, M. Yu, Z. Cao, S. Li and M. Hong, *Cryst. Growth Des.*, 2018, **18**, 2956-2963.

(14). M. J. Frisch, G. W. Trucks, H. B. Schlegel, G. E. Scuseria, M. A. Robb, J. R. Cheeseman, G. Scalmani, V. Barone, B. Mennucci and G. A. Petersson, *Gaussian 09, Revision D.01,;Revision B.01,; Gaussian, Inc.*: Wallingford CT, **2010**.